Journal of Porous Materials (2018) 25:1633–1648
https://doi.org/10.1007/s10934-018-0577-4

Hierarchical porous carbon templated with silica spheres of a diameter of 14 nm from pure chitosan or a chitosan/$ZnCl_2$ solution

Maria Leżańska[1] · Andrzej Olejniczak[1,2] · Jerzy P. Łukaszewicz[1]

Published online: 9 February 2018

Abstract
Nitrogen-containing mesoporous carbons with the use of colloidal silica spheres of (14 nm) and chitosan as a carbon precursor were obtained. A removal of such small template particles from carbonized silica–chitosan composite is difficult and HF with a minimum concentration of 15 wt% should be used. By varying the silica-to-chitosan ratio, the porous characteristic of products is controlled. The modification by $ZnCl_2$ with a molar Zn-to-C (in chitosan mass) ratio of '6' results in the development of microporosity; however it is accompanied by a significant reduction of mesopore volume (V_{mes}). The addition of $ZnCl_2$ in a ratio of '5.25' and pH adjustment to 5.8 increase the volumes of micropores, small mesopores, BET surface area to 1975 m^2/g, and preserve V_{mes} of 4.15 cm^3/g. The novelty of the presented strategy is the creation of microporosity in the hard-templated materials by incorporating $ZnCl_2$ into the mixture of Ludox HS-40 template and chitosan precursor, as well as the investigation on how the pH of synthesis influences the final porosity. The pH of a silica–chitosan–zinc solution, equal to 3.9, provides some coordination of Zn^{2+} by –OH and $–NH_2$ groups, whereas pH adjustment to 5.8 results in the precipitation of a new template—$Zn(OH)_2$.

Keywords Chitosan as carbon precursor · ZnO · Carbon replicas · XPS · Mesoporous materials · LUDOX silica template · Pore generation by $ZnCl_2$

1 Introduction

Hierarchical porous carbons are characterized by well-balanced and usually interconnected micro- and mesopores. All pores of various widths and shapes usually play different roles in its practical application. The mesopores facilitate a rapid transport of ions in electrodes, while micropores provide a large surface area for the accommodation of the charge [1].

Doping carbon with heteroatoms, such as nitrogen, increases its conductivity and results in an improved capacitance of these carbons, mainly due to pseudocapacitance [2]. On the other hand, high-temperature treatment may both destroy mesopores, because of changes in the structure toward graphene rings, and remove a significant amount of nitrogen atoms from the structure. To create a mesopore system of a strictly defined diameter, it is necessary to use either a soft [3, 4] or a hard template [5–7] in the form of ordered porous silica or colloidal silica. The role of the soft template was played by triblock polymers, for example: P123, F127. At the beginning [4, 6], mostly phenolic resins played a role of a carbon precursor. Later on, sugars, eg. glucose, were used. Both types of precursors were successfully used in the synthesis of structured carbons using soft or hard templates [4–7]. In the syntheses of soft-templated carbons, the following precursors were used to introduce nitrogen: resorcinol, urea, and formaldehyde [8], resorcinol/hexamine [9], 3-aminophenol and α-arginine [10].

The use a colloidal silica template in the synthesis of carbon resulted in a material with a large pore volume and uniform mesopores. The beads of colloid silica are available over a wide range of diameters, e.g. (7–100 nm). For example Ludox colloidal silica is marketed as 7, 14, 24 nm-sized,

Electronic supplementary material The online version of this article (https://doi.org/10.1007/s10934-018-0577-4) contains supplementary material, which is available to authorized users.

✉ Maria Leżańska
miriam@chem.umk.pl

[1] Faculty of Chemistry, Nicolaus Copernicus University, Gagarina 7, 87-100 Torun, Poland

[2] Flerov Laboratory of Nuclear Reactions, Joint Institute for Nuclear Research, Dubna, Russia 141980

thus a template molecule of the appropriate diameter can be provided and tailoring the pore size of carbon seems to be feasible. In the first work on obtaining carbons using colloidal silica [5], a pore diameter of 12 nm, was used. The diameter of the carbon pores did not exactly match the diameters of the silica spheres. However, in a later work [6], the material whose pore size reflected the diameter of the particles of the template, was obtained from the same precursor. Carbon–silica composite is subjected to silica etching with hydrofluoric acid or NaOH, which does not seldom affected the order of material. It was shown by Choma et al. [11] that HF was more efficient as an etching agent in comparison to NaOH solution.

Hard-templating methods have already used various precursors, for example, melamine [12, 13] or 1-ethylmethylimidazolium dicyanide ionic liquid [14]. The use of nitrogen-containing hierarchical carbons potentially involves two areas: electrochemistry, because they form electrodes for supercapacitors or for usage in oxygen reduction processes [15], and as sorbents for CO_2 retention. This latter application most often involves nitrogen-free adsorbents, in which strongly developed pores nitrogen-containing molecules can be adsorber, e.g. the carbon prepared from resorcinol and formaldehyde precursors and Ludox, was impregnated with polyethyleneimine [16]. It is also important to mention here that the carbon obtained from glucose and Ludox, was impregnated after the synthesis of aminophenol [17]. These ice-templated and hard-templated materials which have shown an area of up to 2096 m^2/g and a pore volume of 11 cc/g were tested for both CO_2 adsorption and in supercapacitors.

In such a mesoporous system, micropores may be produced, by known activators, such as $ZnCl_2$ [18] or, for example, TEOS [19], added directly to the mixture during synthesis. It is possible to modify the hard precursor by means of physical activators (e.g. CO_2) [20] or chemically, with ie, KOH [21–23] or $ZnCl_2$ [24–28] after pre-carbonization.

Salt templating involves the impregnation of carbon precursor with salt or incorporation of it into the mixture during synthesis, precipitation from the solution, and carbonization of carbon precursor around nano-pools at high temperature. Mainly micropores and small mesopores are generated after washing of salt particles. The presence of $ZnCl_2$ ensures a higher degree of carbonization of the glucose–silica composite [18]. An interesting synthesis approach, which consisted of hard templating with colloidal silicas and salt-templating by $ZnCl_2$ and glucose as a carbon precursor, in some cases completed by physical activation with CO_2, resulted in the trimodal porous carbon. The pores of a diameter of ca. 2, 12 and 28 nm were generated in a single material [18]. The physical activation with CO_2, resulted in a substantial increase of microporosity and as a result BET surface area up to ca. 2500 m^2/g.

In this case, salt templating could translate into both high energy density and high capacitance retention capability when materials are used as electrodes for supercapacitors. The high capacitance retention at a very high current density of 40 A/g, of ca. 87% was obtained when 'hard-templated' mesopores were presented in carbon materials [18].

The ZnO was tested both as a template and as an activator [29, 30]. In 2016, facile synthesis of nitrogen -doped hierarchical porous carbons with a high surface area have been shown in [29]. The obtained carbons possessed high surface area of 2412 m^2/g and large pore volume of 3.436 cm^3/g. However, the yield of carbon seems not to be sufficiently high. Carbonization yielded micropores from boiling of $ZnCl_2$ at approximately 283–293 °C. Thus, the carbonization temperature of 900 °C is high enough to remove traces of $ZnCl_2$ or ZnO species from the carbon material and no leaching by HCl is necessary.

Depending on pH, zinc chloride can interact with chitosan in different ways, during synthesis. It is likely that these conditions, which provide a large proportion of Zn^{2+}, allow a similar effect of $ZnCl_2$ as in the case of the previously studied hard lignocellulosic materials: Zn^{2+} is not strongly bound to chitosan, into the complex by $–NH_2$ or –OH groups. The Zn^{2+} cations complexed with aminocarboxylates were homogenously distributed in the material on the molecular level, during synthesis of microporous carbons [31].

The aim of the study is to control the micro/mesoporosity of carbons obtained from chitosan by: (i) changing the silica-to-chitosan ratio, (ii) using the pH changes that provide the addition of different amounts of $ZnCl_2$ and LUDOX. In this study, the carbon material was obtained with spheres of a silica template of a 14 nm-diameter. We used smaller silica spheres as compared to those used in the previous paper (24 nm) [32]. The pores of 24 nm in some cases can be too large to align 8–10 nm diameter nanoparticles in a perfect manner. A transport of molecules can be too fast in such large pores, as well. The aim of the work is to develop a microporous structure without destroying the mesopores. However, in the previous series of samples fabricated using 24-nm-diameter silica particles—CAS-40 [32], the materials characterized with the highest mesopore volume had very thin walls of 0.61–0.64 nm, e.g. synthesized at the SiO_2 to chitosan mass ratio of 1.75. The formation of additional small-diameter pores in such thin walls due to the action of $ZnCl_2$ activator during carbonization at high temperature may bring about a collapse of the structure. Hence, in the previous work [33], for modification with $ZnCl_2$ the ratios of silica to chitosan of 1.0 and 2.5 were selected. Given, analogous concentrations of chitosan and both Ludox silicas in the synthetic mixtures, and comparable density of those latter, the materials with the highest pore volume, for the same silica to chitosan ratio could be expected. The material

obtained by using Ludox HS-40 will probably have pores of a smaller diameter, which may suggest a greater order of spherical pores and consequently higher mechanical resistance. A chitosan-to-Zn^{2+} ratio influences the interaction of Zn^{2+} and chitosan. Chitosan is a natural biopolymer from a renewable source. Chitosan-derived carbons are appreciated for the high content of nitrogen that can be introduced into the material [32]. Previously, we presented some exemplary applications of chitosan in the chemistry of carbon materials [32, 33]. It is important to investigate the effect of the amount of $ZnCl_2$ and the temperature of carbonization on the final nitrogen content of the samples. The novelty and the main difference between the standard modification of carbon material with $ZnCl_2$ and that used in this work, is that the carbon or precarbonized precursor is not impregnated with the salt, but $ZnCl_2$ is incorporated into the solution during the synthesis, as it was mentioned in our previously presented work [33].

The synthesis with a $ZnCl_2$ activator in solution enables other modifications to be applied to solutions, including pH adjustments.

2 Experimental

2.1 Sample preparation

The chitosan–silica composites were prepared by a solvent evaporation technique, as described in Ref [32]. The silica-to-chitosan ratio was maintained within a range of 1–3.10. The designated amount of a colloidal silica solution (Ludox HS-40) was added dropwise and under continuous stirring to a 100 g of a 0.5% (w/v) chitosan solution in 1% (w/w) aqueous acetic acid. However, a pH of the synthetic mixture of selected samples was modified by adding dropwise the ammonia solution with the molar concentration of 0.1 mol/l, under vigorous stirring, up to the value of 5.8. The obtained thick slurry was transferred to Petri dishes. After the evaporation of the solvent, the semitransparent films of the composite were carbonized under Ar at 900 °C for 4 h. The heating rate was 0.5 °C/min. The weight of films was carefully controlled before and after carbonization. Removal of the silica template was done by washing twice with a 10 wt% HF solution in acetone/water. The carbons were next washed thoroughly with an acetone–water mixture until the conductivity of the filtrate became 10 μS. In some cases, an additional washing in 15 wt% HF was applied to accomplish the removal of the template. The carbon materials washed with 10 and 15 wt% HF were designated as CHS40-Xow and CHS40-X, respectively, where X denotes the silica-to-chitosan mass ratio.

To generate microporosity, $ZnCl_2$ with an approximate molar Zn-to-C (in chitosan mass) ratio within the range of 1–6, was added to the chitosan solution and sonicated. The series synthesized with $ZnCl_2$ was carbonized, as described above. In the case of materials modified with $ZnCl_2$, only a single stage of SiO_2 removal in 10 wt% HF solution was sufficient.

Various types of composites were examined in this work. The following exemplary names of composites of the silica-to-chitosan mass ratio of 1 and molar Zn-to-C in chitosan mass ratio of 4: CHS40-1.00k, CH_Zn4, and HS1_Zn4k corresponded to chitosan/silica, chitosan/$ZnCl_2$, and chitosan/silica/$ZnCl_2$ composites, respectively. The following nomenclature of the samples have been used (Table 1):

The digits '40' were omitted in the name of CHS40-1.00k in Figs. 10 and 11, for clarity.

2.2 Methods

Nitrogen adsorption/desorption isotherms were measured at − 196 °C with the use of an automated volumetric analyzer (ASAP2010, Micromeritics). The micropore and mesopore volumes were calculated by the α_s-plot with non-graphitized soot as a standard. The mesopore size distributions were obtained by BJH-KJS method [34], whereas the distributions of the size of pores within the diameter up to 3.2 nm were calculated by Do's method optimized by ASA algorithm [35–37].

Total carbon, hydrogen, and nitrogen contents were determined by elemental analysis (Vario MACRO CHN, ELEMENTAR Analysensysteme). Thermal analysis was performed using STA 449 FS NETZSCH, (Thermal Analysis supported DSC) within the temperature range of 20–1000 °C. The thermogravimetric studies of carbons were carried out in an air atmosphere at a heating rate of 5 °C/min, whereas chitosan and composites (chitosan–$ZnCl_2$, chitosan–silica, chitosan–$ZnCl_2$–silica) were analyzed under N_2 at a heating rate of 10 °C/min.

Table 1 Nomenclature of exemplary samples

Synthesized	Composites before carbonization	Composites after carbonization and partial removal of SiO_2	Carbons
Without $ZnCl_2$	CHS40-1.00k	CHS40-1.00ow	CHS40-1.00
With $ZnCl_2$	HS1_Zn4k	–	HS1_Zn4

(4 denotes Zn/C ratio)

The chitosan and its composites as foils were analyzed with a Bruker Optik Gmbh 2014 FTIR spectrometer, model VERTEX 70v. The resolution for each spectrum was 2 cm^{-1}.

The aim of X-ray photoelectron spectroscopy study was a determination of the elemental contents at the surface of carbon samples and the contribution of surface groups to surface species. The XPS measurements were performed using a K-alpha (Thermo Scientific) spectrometer. The incident radiation was Monochromatic Al Kα X-rays (1486.68 eV) at the lamp working parameters of 12 kV, 3 mA. The diameter of analyzed area was 400 µm. The base pressure in the analysis chamber was 7×10^{-10} mbar and during sample analysis it was kept within a range of 1×10^{-9}–9×10^{-9} mbar. Survey scans were carried out over 1200–10 eV binding energy range with 0.5 eV ramp at analyzer pass energy of 200 eV. Narrow high-resolution scans were run with 0.05 eV steps at analyzer pass energy of 20 eV and 50 ms dwell time.

X-ray diffraction (XRD) analysis of the carbonized film was performed using a PANalytical X'Pert PRO powder diffractometer with Cu K_radiation (40 kV, 30 mA).

The specimen morphology was studied using a Tecnai G2 (FEI) microscope operating at 200 kV with energy dispersive X-ray analysis (EDX).

3 Results and discussion

3.1 Characterization of porosity

Firstly, we discuss the pours characteristic of the carbon replicas prepared by double-washing in 10 wt% HF. The N_2 sorption isotherms of type IV according to IUPAC classification of: CHS40-1.00ow and CHS40-1.75ow, characterized with hysteresis loop of type H1 and of CHS40-2.50ow and CHS40-3.10ow, which exhibited complex hystereses of H1–H5 types [38], are presented in Fig. 1. The amounts of adsorbed N_2 are significant in case of CHS40-1.00ow, CHS40-1.75ow, and CHS40-3.10ow as opposite to that of CHS40-2.50ow. The V_t of this sample is 0.49 cm^3/g (Table 2) only. It can be asked if an ordered structure with developed porosity is able to be created at the SiO_2-to-chitosan mass ratio of 2.50? According to our previous results, concerning the synthesis of carbons using chitosan and Ludox AS-40 silica template [32] the SiO_2-to-chitosan ratio above which the structure was overloaded with silica equaled 3.10. The smaller silica spheres of Ludox HS-40 can more effectively fill the space, as compared to Ludox AS-40, thus, the more ordered porous system can be generated in the sample synthesized at SiO_2-to-chitosan ratio of 2.5. The synthesis of the material at a silica-to-chitosan ratio of 3.10 was carried out so. There is a wide hysteresis loop on the isotherm that begins at 0.4 p/p_s. The gradual uptake of the adsorption branch of the isotherm at a pressure range of 0.40–0.95 p/p_s suggests a broad pore size distribution (Fig. 1 d).

An increase in the silica loading exerts a detrimental effect on the porosity of the obtained carbon. The pore size distribution of CHS40-3.10ow was shifted to lower diameters, because carbon prepared from overloaded composite did not exhibit mesopores of the diameter related to silica template particles (Figs. 2, S1 Online Resource 1), as in the case of the sample CAS40-3.10 [32] synthesized using Ludox AS-40 and at silica-to-chitosan ratio of 3.10.

The low volumes of pores of CHS40-2.50 could only be explained by the fact that the pores of the material are filled with something. To do this, a thermal analysis of the samples in the air was performed. The TG curves in air of these composites, shown in Fig. 3, exhibited the most abundant weight losses within the range of temperature of 500–650 °C for all the carbons studied. However, the weights of residues after burning significantly differ from each other. The total weight loss for the sample CHS40-3.10ow was 98.4% whereas for the samples synthesized at a lower SiO_2/chit ratio of 1, 1.75, and 2.50 the losses reached 90.8, 73.0, and 21.6% respectively.

Thus, the examined samples were etched with HF once again, but the concentration of HF was increased up to ca. 15%. It resulted in the increase of the pore volume in the series $V_{CHS40-1.00} < V_{CHS40-1.75} < V_{CHS40-2.50}$, which corresponded to the amount of silica removed. The N_2 adsorption isotherms preserve their type after the second washing. The second washing resulted in a significant increase of V_t of CHS40-2.50. The pore volume of CHS40-2.50ow do not exceed 0.5 cm^3/g whereas after second washing reached 2.70 cm^3/g (Table 2). Second washing did not cause the maxima of the PSD to be shifted.

The carbon spheres and flat circle objects (Fig. 4) can be found in TEM images of the best-ordered CHS40-1.75 sample (b, d) and its composite (a, c), respectively.

The silica was relatively easily removed from the CHS40-1.75-ow sample after the first wash, as this material probably exhibits a higher pore volume and surface area as it is characterized by the presence of a thinner wall. The sample synthesized using LUDOX AS-40, obtained at a SiO_2/chit ratio of 1.75 exhibited the thinnest pore wall (0.61 nm) among all the studied carbons [32]. Thicker walls and a greater volume of the walls relative to the pore volume in the sample require the use of more concentrated HF and more drastic leaching conditions. The steep capillary condensation step (Fig. 1) at very high p/p_0 of ca. 0.85 confirms the existence of large mesopores in twice-washed samples CHS40-1.00, CHS40-1.75, and CHS40-2.50. The hysteresis loop of the H1 type well defines cylindrical mesopores or approximately uniform spherical ones, with the large enough windows connecting them. A high sorption capacity confirms that pores are connected.

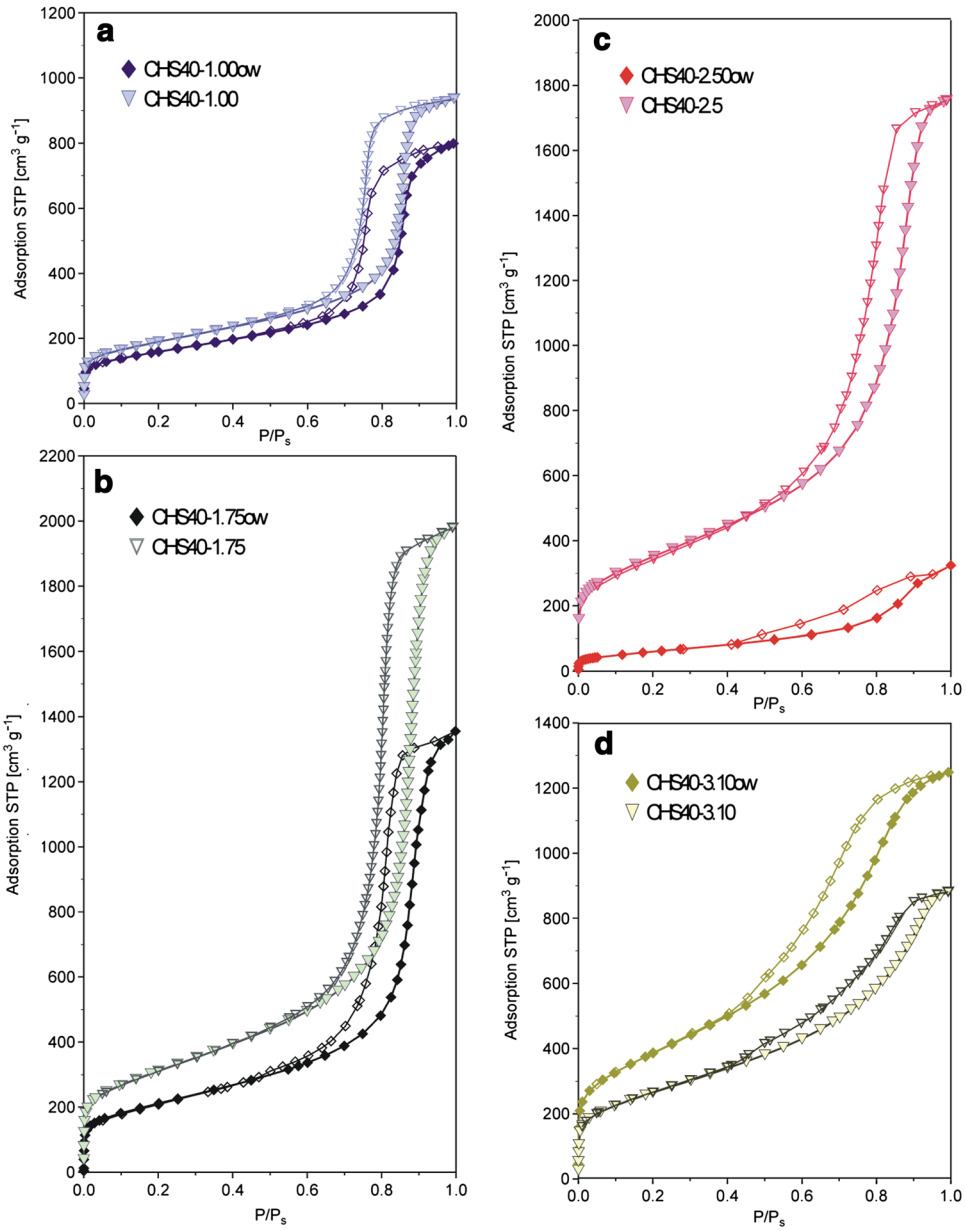

Fig. 1 Nitrogen adsorption–desorption isotherms of carbon samples: CHS40-1.00 (**a**), CHS40-1.75 (**b**), CHS40-2.50 (**c**), and CHS40-3.10 (**d**), once or twice treated with HF

On the other hand, the sample of CHS40-3.10ow, being characterized with not uniformly shaped pores and hardly any silica residue probably partially collapsed after second washing (Fig. 1 d). In this case, the amount of carbon precursor is insufficient to form well-defined carbon walls. The rewashing of the structure with HF causes its destruction.

Since the nearly mesoporous carbons were obtained using Ludox HS-40 silica template we used $ZnCl_2$ to develop the microporosity. Numerous hard, partially carbonized or raw precursors of carbon, e.g. lignocelulitic materials (coconut shells and palm seeds [25], pistachio-nut shell [24], peach stones [40]) were impregnated with various amounts of $ZnCl_2$, which was used to generate the abundant volume of micropores in the carbonaceous materials after activation. For these impregnated samples, the zinc chloride assumes a dehydration agent role [24, 39]. It decomposes under the conditions of carbonization when heated under N_2 or vacuum at high temperature. With $ZnCl_2$ impregnation, the formation of tars and any other lignin fragments that may clog the pores is inhibited [24, 40] and the movement of the volatiles through the pore passages will not be hindered and they will be subsequently released.

The initial increase in $ZnCl_2$/precursor mass ratio up to 0.75 is usually to limit the release of volatile matter, which results in the increase of the yield of microporous carbon. However, further growth in the mass ratio above 0.75 results in the non-hindered release of volatiles accompanied by a continual decrease in the yield of activation under N_2, and

Table 2 Elemental bulk and surface composition and some textural parameters of chitosan-derived carbons

Sample	S_{BET} (m^2/g)	V_t (cm^3/g)	V_{mi}[a] (cm^3/g)	V_{mes}[a] (cm^3/g)	d_p (nm)	EA		XPS		
						N (wt%)	N/C	N (at.%)	O (at.%)	N/C
CHS40_1.00ow	559	$1.23^{0.99}$	0.031	1.15	15.5/2.93	n.d.	n.d.	n.d.	n.d.	n.d.
CHS40_1.75ow	749	$2.08^{0.99}$	0.021	1.95	17.3/2.82	n.d.	n.d.	n.d.	n.d.	n.d.
CHS40_2.50ow	220	$0.49^{0.99}$	0	0.352	13.5/3.02	n.d.	n.d.	n.d.	n.d.	n.d.
CHS40_3.10ow	1381	$1.93^{0.99}$	0.084	1.84	3.25	n.d.	n.d.	n.d.	n.d.	n.d.
CHS40_1.00	666^5	$1.45^{0.99}$	0.049	1.38	15.6/2.93	7.27^5	0.072	n.d.	n.d.	n.d.
CHS40_1.75	1103	$3.06^{0.99}$	0.034	2.91	17.8/3.21	6.06^5	0.061	4.67	6.06	0.052
CHS40_2.50	1248	$2.70^{0.98}$	0.047	2.61	15.0/3.20	5.89	0.059	n.d.	n.d.	n.d.
CHS40_3.10	947	$1.36^{0.99}$	0.036	1.27	2.91	6.16	0.069	n.d.	n.d.	n.d.
HS1_Zn4	1216^5	$1.71^{0.99}$	0.374	1.26	18.8	5.37^5	0.054	4.30	8.47	0.049
HS1_Zn6	1430	$1.42^{0.99}$	0.424	0.577	~15	6.83	0.105	n.d.	n.d.	n.d.
HS1.75_Zn2	1229	$3.08^{0.99}$	0.216	1.90	20.2	4.16	0.042	4.89	7.28	0.056
HS1.75_Zn4	1770^5	$3.23^{0.99}$	0.354	2.41	20.0	4.26^5	0.043	n.d.	n.d.	n.d.
HS1.75_Zn6	1326	$1.67^{0.995}$	0.413	1.02	~20	3.87	0.050	3.07	8.49	0.035
CHS40_1.38	1085	$4.02^{0.98}$	0.125	n.d	2.91/broad	4.53	0.054	n.d.	n.d.	n.d.
HS1.38_Zn4	1536	$2.97^{0.99}$	0.317	1.90	15–33	4.18	0.048	n.d.	n.d.	n.d.
HS1.38_Zn4pH5.8	1718	$3.33^{0.98}$	0.338	3.16	~2/18.0	7.30	0.087	n.d.	n.d.	n.d.
HS1.38_Zn5.25pH5.8	1975	$4.15^{0.985}$	0.173	3.42	2.62/15–30	4.15	0.048	n.d.	n.d.	n.d.

V_t single point pore volume (measured at the partial pressure indicated italics), V_{mi} volume of micropores, V_{mes} volume of mesopores, d_p pore diameters derived from the adsorption branch by the BJH-KJS method, *a* obtained from α_s-plot analysis using N_2 adsorption data of BP280 carbon black as reference [39] results presented in the reference [39]. *n.d.* not determined

at the $ZnCl_2$/precursor ratio of 1.5, the carbons are mostly mesoporous [24]. Various limit ratios of $ZnCl_2$/precursor mass of 1.0 [40] and 1.5 [27] above which predominantly mesoporous carbon is obtained, was revealed in other works. The $ZnCl_2$ to sludge ratios less than 1.0 and higher than 3.5 resulted in the production of microporous and 80% mesoporous carbon, respectively [27]. To produce micropores in the materials studied in this work, the composition of the reaction mixture was modified during the syntheses by various quantities of $ZnCl_2$. Systematic studies on the effect of $ZnCl_2$ on the porosity of materials were conducted for two silica-to-chitosan ratios, i.e. 1.00 and 1.75 (Figs. 5, S2 Online Resource 1). The non-modified $ZnCl_2$ materials obtained for these ratios were characterized by the best structural order. The addition of $ZnCl_2$ reduced the carbonization yield for both tested silica-to-chitosan mass ratios (Fig. 6). The molar Zn-to-C in chitosan mass ratio of 4 corresponds to $ZnCl_2$/chitosan mass ratio of ca. 1.42. The adsorption isotherm of parent samples and these modified with small amounts of $ZnCl_2$ reveal condensation in the pores accompanied by hysteresis in the relative pressure p/p_0 range from 0.60 to 0.95 (Figs. 5 and S2 in Online Resource 1), indicating filling of the primary mesopores. When the amount of $ZnCl_2$ increases up to 4 the hysteresis broadens and cover the range of 0.4–1.0 (Figs. 5, S2 in Online Resource 1). Secondary mesoporosity is also observed, which may include the holes in the walls and interparticle voids. The isotherms of CHS40-1.00 and CHS40-1.75 samples are terminated perpendicular to y axis, whereas those of $ZnCl_2$-modified samples asymptotically approach y-axis and do not exhibit any plateau at $p/p_0 \sim 1$. Those features correspond to Type II b isotherm and loop of H3 type which can be obtained with materials if the pore network consist of macropores incompletely filled with condensate [38].

At the beginning, with the increase in $ZnCl_2$ content in both silica-and-chitosan ratios, the small growth of microporosity is accompanied by a slight decrease in the content of mesopores (Tables 2 and S1 in Online Resource 1). The Zn-to-C ratio of 2.00 is similar to the mass ratio of ca. 0.71. The diminished yield of carbon at Zn-to-C ratio of 4.00 for both series is accompanied by an increase in mesoporosity. Thus, 4.00 is just that value at which a formation of additional mesopores is observed, which can be referred mass ratio of 1.42–1.50 in the literature. The micropore and mesopore volume were calculated by the α_s-plot. It is difficult to find models, which do not account for the effect of mesoporosity on the determination of micropore size. It has been shown that for $ZnCl_2$ modification the activated carbons obtained contain large amounts of small mesopores of the diameter of 2.0–3.2 nm. The micropore and small mesopore size (up to 3.2 nm) distributions were obtained by [35–37], which assumes the slit-like shape of the pores (Fig. 7). However, the distributions of the size of primary mesopores resulted from templating, were determined using the BJH-KJS model

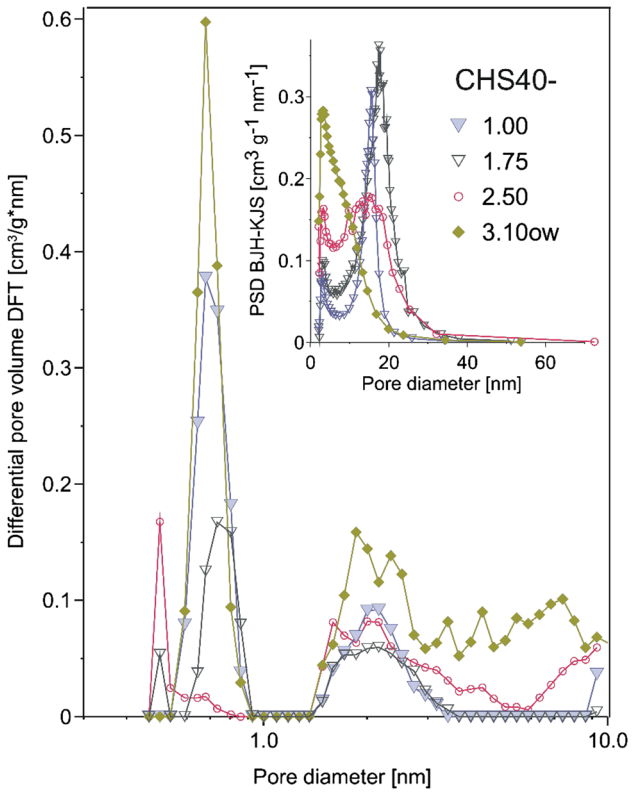

Fig. 2 Micro-mesoporous size distributions obtained by Do's method (optimized by ASA algorithm) and mesopores size distributions obtained by BJH-KJS using adsorption results—(inset), of carbons synthesized at various silica-to-chitosan ratios

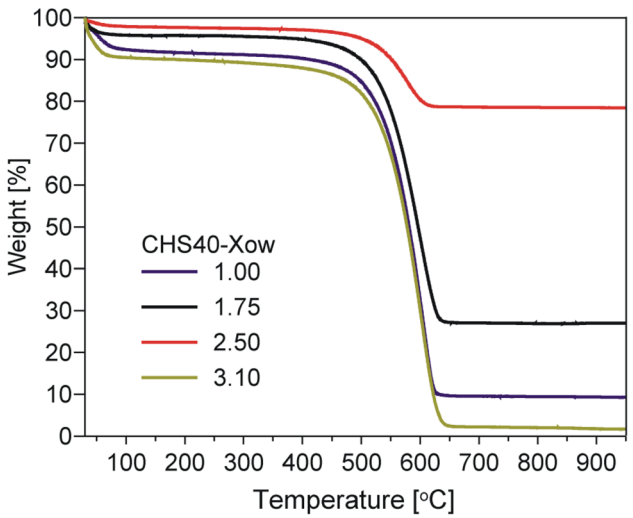

Fig. 3 The thermogravimetric profiles of silica–carbon composites in air, once washed in HF (CHS40-Xow)

[34]. This approach does not impose the need to cut the peak, which extends up to about 3.2 nm, in the proximity of its maximum at 2 nm and allows to estimate a contribution of effective pores created as the concentration of the $ZnCl_2$ modifier increases. Cumulative volumes of pores characterized with the diameters of up to 0.8, 1.0, and 3.2 nm, were presented in Table 3. The KJS correction eliminated this problem in the case of perfectly cylindrical homogeneous materials—MCM-41 [34]. This amendment was also applied to cubic materials FDU-12 [41], containing spherical pores, which can be imagined as cube corners that are connected by cylindrical pores of smaller diameter. This type of structure exhibited fluid cavitation in the pores; if the difference between sphere size and input window is large enough, and entry windows sizes less than 4–4.5 nm could cause emptying of pores under pressure higher than that for typical desorption from such windows ($p/p_0 \sim 0.4$) [41, 42]. The width of cylindrical pores, in the materials studied in this work, corresponds to the diameter of balls in the rows, which, in addition, are arranged in three dimensions. However, the depth at which a space of one sphere in the structure would overlap with that of the other is enough that the window diameter is not much smaller than the sphere diameter. Thus, no cavitation effects are observed in non-modified CHS40-type carbons. The rise of the $ZnCl_2$ concentration up to molar Zn-to-C in a chitosan mass ratio of 4 for CHS40-1.75 creates additional mesopores of the diameter bigger than ca. 20 nm, whereas in the case of CHS-1.00 resulted in widening of primary mesopores. The ratio of $ZnCl_2$ to chitosan affected BET surface area, as well. Except the highest $ZnCl_2$ concentration for both the series; the higher the salt content, the more developed the surface. Increasing the impregnation ratio produces similar trends for $S_{BET,}$ V_t, and V_{mes} in the series HS1.75_Znx (Tables 2, S1 in Online Resource 1). It can be concluded that the modification with a high $ZnCl_2$ content results in a substantial collapse of the primary mesopores (Table 2). The shape of the N_2 desorption isotherm for samples modified with the highest amounts of porogen: HS1_Zn4, HS1_Zn6, and HS1.75_Zn6 implies cavitation (Fig. 5). The desorption of HS1_Zn4 sample is step-wise (Fig. 5). This kind of isotherm was measured for plugged hexagonal templated silicas, containing both open and encapsulated mesopores. During the desorption of N_2 encapsulated mesopores empty at lower pressure than the open pores of similar size [42, 43]. The pore blockage is due to partial collapse of the materials' walls during modification with $ZnCl_2$.

To generate micropores while preserving a large V_{mes}, the ratio of silica to chitosan in the mixture was reduced to 1.38, while keeping the molar Zn-to-C (in chitosan mass) ratio of 4 (HS1.38_Zn4). The micropore volume was significantly increased and reached 0.317 cm^3/g (Table 2), (the results resulted from N_2 adsorption isotherm, presented in Fig. 8). A further rise in V_{mi} was achieved after increasing the pH of the synthetic mixture of HS1.38_Zn4 up to 5.8 (sample HS1.38_Zn4pH5.8). The data from N_2 adsorption isotherms

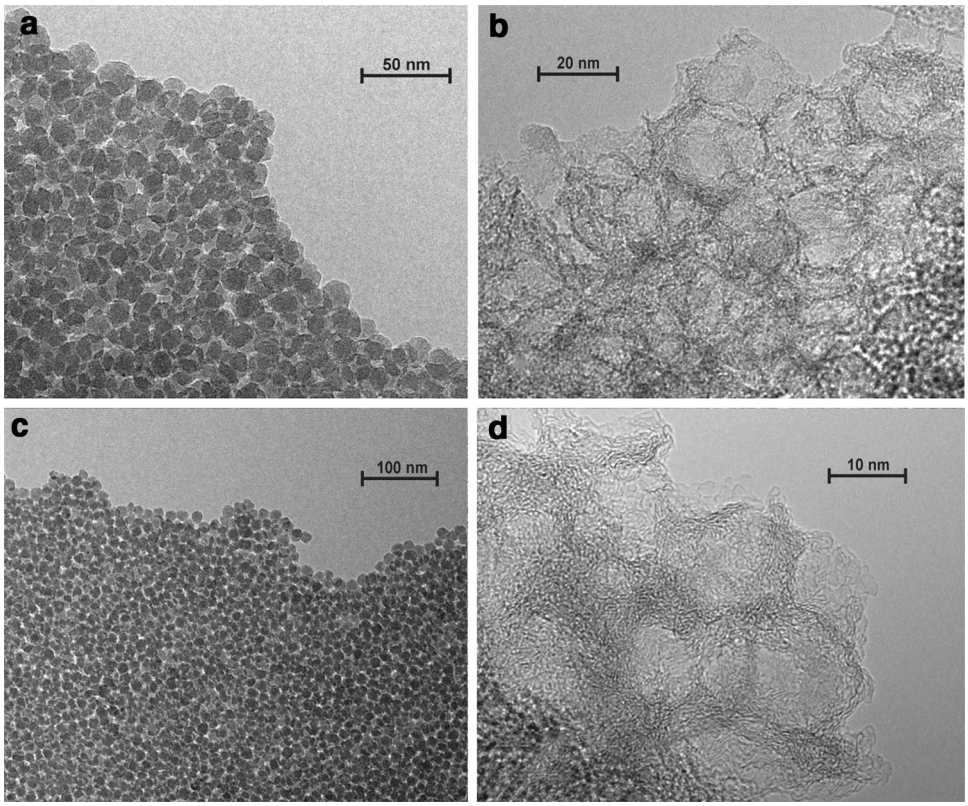

Fig. 4 TEM micrographs of chitosan–silica composite of CHS40-1.75k in (**a**, **c**) and of CHS40-1.75 carbons in (**b**, **d**) respectively

(Fig. 8; Table 1) confirm that when a higher Zn-to-C ratio of 5.25 and a pH adjustment were used, the BET surface area of resulted sample developed to 1975 m^2/g and volume of small mesopores of the diameter of ca. 3 nm increased, while microporosity diminished (Fig. S3 in Online Resource 1). The addition of $ZnCl_2$ to the synthetic mixture and the pH adjustment results in carbon materials of disordered morphology. The irregular pseudo-spherical particles can be seen in the TEM images (Fig. 9 a–f) of studied samples. The Zn^{2+} concentration and pH are factors that affect precipitation of $Zn(OH)_2$, and indirectly influence the porosity of the resulting material. The precipitation of $Zn(OH)_2$ and transformation of it will be discussed in Chap. 3.2.

The XPS analysis (Table 2) has shown the templated carbons contain Si, Zn, Cl and S impurities in amounts up to 0.14, 0.08, 0.10, and 0.40 at.%, respectively. The trace amounts of Si confirm the effective removal of the template from the pores of the material, whereas the Zn and Cl traces indicate almost complete removal of $ZnCl_2$. The addition of ever greater amounts of $ZnCl_2$ results in an increase of oxygen contents, which is accompanied with a nitrogen content decrease in the carbon materials. A comparison of XPS data of CHS40_1.75 with those of $ZnCl_2$- modified samples suggest that a local higher $ZnCl_2$ concentration contributes to the removal of N heteroatoms. For the samples loaded with the highest $ZnCl_2$ amounts, the contents of N and O obtained from elemental analysis, are higher as compared to those of revealed by XPS. Thus, their concentration can be surmised lower in the near surface region in comparison to the bulk. The opposite trend for the composite of the sample HS1.75_Zn2 can be explained by the fact that it is characterized by a quite low concentration of $ZnCl_2$, which has to be uniformly distributed.

The TEM/EDX analysis of the sol formed during synthesis of HS1_Zn4k (Fig. S4 in Online Resource 1) suggests the uniform distribution of all heteroatoms in the chitosan–silica–zinc composite. The carbonization of the materials obtained at SiO_2/chitosan mass ratio of 1.38 and 1.75 and of those prepared in the presence of $ZnCl_2$ resulted in the slightly higher removal of nitrogen from the structure (Table 2). However, the reason for the relatively high nitrogen content in the HS1.38Zn4pH5.8 sample, in comparison to those in other $ZnCl_2$-modified carbons, has not been explained yet. However, Zn can exist as cations or can be precipitated in $Zn(OH)_2$ at the pH 5.8. The high $Zn^{2+}/Zn(OH)_2$ ratio may both cause more extensive nitrogen removal and lead to more disordered structure. The sample containing 7.30 wt% of nitrogen (HS1.38Zn4pH5.8) is characterized by monomodal pore size distribution (Fig. 8) and the most ordered structure among $ZnCl_2$-modified samples, as shown in Figs. 8 and 9. Hence, the concentration of OH^- anions at the pH 5.8 was probably not sufficient to precipitate as much Zn^{2+} cations as $Zn(OH)_2$ when molar Zn-to-C ratio was kept 5.25.

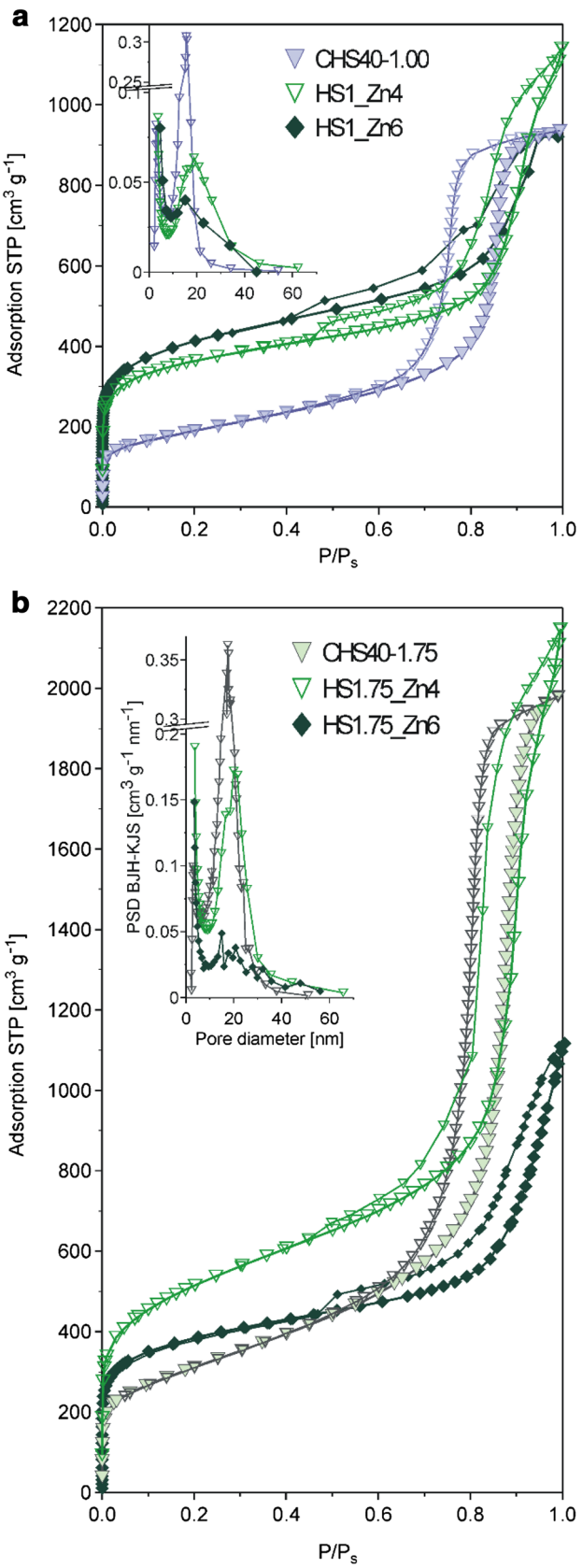

Fig. 5 Nitrogen sorption–desorption isotherms and BJH-KJS pore size distributions (adsorption) for $ZnCl_2$ modified mesoporous carbons of HS1_ZnY (**a**) and HS1.75_ZnY (**b**) types. The results for parent samples (non-modified—CHS40-1.00 and CHS40-1.75, respectively) were presented for comparison

3.2 TGA analysis

The TG and DTG results confirmed the two-stage process of decomposition of chitosan as well as chitosan-silica composite CHS40-1.00k (Fig. 10 a). The maximum of the first DTG peak at ca. 100 °C in the curves of all the carbons studied can be attributed to the loss of water. The main peak situated within the range of temperature 180–340 °C [44], can be attributed to the glass transition of chitosan and subsequent degradation of the main chain of chitosan [45]. The most important half-products of the pyrolysis of chitosan are pyrazines [45]. Hence, the α-aminocarbonyls, obtained from the decomposition of chitosan, are considered to be their precursors [46]. The α-aminocarbonyls react with each other to form pyrazines. A thermal degradation started with the scission of a C–O–C bond [45, 47], which generates CO_2, oligomers, dimers of glucosamine and solid char [48]. The latter releases ammonia and acetic acid.

Compared with chitosan, the decomposition of the chitosan–Zn complex should be easier and more thorough [45]. If the pH during the synthesis of the chitosan–zinc–silica composite was not adjusted, it remained acidic and not so high that chitosan–Zn complex could be created [45, 49]. The degradation of chitosan–$ZnCl_2$ and chitosan–silica–$ZnCl_2$ composites (Fig. 10 c–f) involves three stages. The first peak in DTG curve can be referred to water loss, whereas the second one to chitosan chain degradation which comes and ends at the range of temperatures of 160–280 °C, slightly lower as compared to pure chitosan. The dehydrating agent—$ZnCl_2$ probably enhances degradation. The more abundant content of $ZnCl_2$ in the composite (Fig. 10 c, d) as compared to (Fig. 10 e, f) results in a shift of the peaks to the lower temperature. Moreover, a maximum of degradation of chitosan-derived biochar at the presence of $ZnCl_2$ corresponds to 545 and 525 °C for chitosan–zinc–silica (HS1_Zn4k) and chitosan–zinc (CH_Zn4) composites, respectively. It has been shown that the condensation of glucosamine can be catalyzed by granulated Zn in the char [50]. The third peak corresponds to the transformation of semi-products, which are similar to those in case of decomposition of pure chitosan; however, their distribution depends on the temperature and time of the reaction [45], and possibly on $ZnCl_2$ content. The role of $ZnCl_2$ as dehydrating agent revealed at various temperatures. The melting point and boiling point of $ZnCl_2$ are at 293 and 732 °C, respectively [51]. A decay of hard raw materials containing cellulose

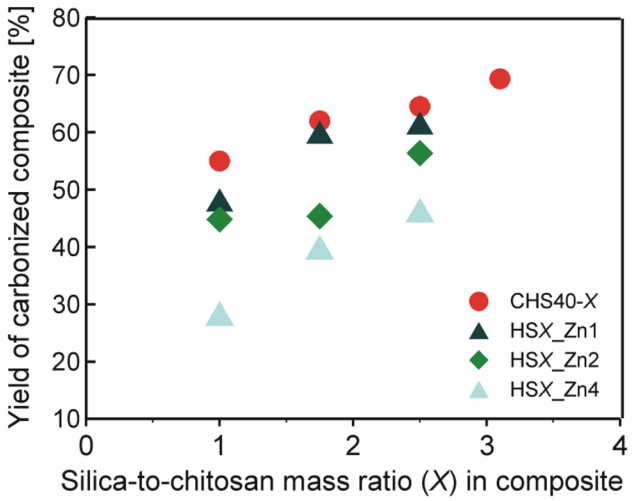

Fig. 6 Yield of carbonized composite (k-type samples) in molar Zn-to-'C in chitosan' ratio, for various silica-to-chitosan mass ratios

Table 3 The volumes of micropores of various sizes

Sample	$V_{cum} \leq 0.804$	$V_{cum} \leq 1.001$	$V_{cum} \leq 3.181$
HS1_Zn1	0.1123	0.1263	0.2086
HS1_Zn2	0.0942	0.1035	0.2066
HS1_Zn4	0.1394	0.1544	0.3121
HS1_Zn6	0.2030	0.2156	0.4525
HS1.75_Zn2	0.0652	0.0747	0.1589
HS1.75_Zn4	0.0823	0.0983	0.2274
HS1.75_Zn6	0.1642	0.1719	0.3504
HS1.38_Zn4pH5.8	0.0804	0.0820	0.1940
HS1.38_Zn5.25pH5.8	0.0525	0.0540	0.2000

and lignin at the presence of $ZnCl_2$ finishes at ca. 700 °C [26]. The transformation of Zn^{2+} complex with much softer chitosan is practically terminated within the range of temperature of 550–600 °C [45, 52], and in this work, chitosan–Zn^{2+} composite decomposes up to 650 °C.

The TG and DTG curves of chitosan–$ZnCl_2$ composites (Fig. 10c–d) have shown that the higher is the salt content, the lower is the yield of carbon. The yields of ~ 18 and 25% for CH_Zn4 and CH_Zn1 were obtained, respectively. The same trend occurs for chitosan–$ZnCl_2$–silica composite (c, d). However, the contribution of silica in the composite is minimum 35%. The yields of carbons obtained at various silica-to-chitosan ratios and $ZnCl_2$ contributions are presented in Fig. 6. The amounts determined by the differences of the masses of samples before and after carbonization under Ar at 900 °C were significantly higher. The very high heating rate during TGA analysis as compared to carbonization, 10°C/min and 0.5 °C/min, respectively, is a probable reason for that discrepancy. Because of that, $ZnCl_2$ probably decomposes at a temperature higher than ca. 650 °C under the conditions of carbonization.

As it was mentioned above, the pHs of chitosan and chitosan–$ZnCl_2$ solutions were 3.4 and 3.3, respectively, and increased up to 3.9 after silica template addition, for the samples obtained at a silica-to-chitosan ratio of 1–1.75. At highly acidic conditions (pH 2) the amino groups of chitosan are fully protonated, while no negative charge in any functional group existed [53]. An electrostatic repulsion may occur between cationic metal ions and positively charged $–NH_3^+$ groups of chitosan at low pH. Therefore, the only interaction which may exist, is the chelation (and this in low percentage) among amino and hydroxyl groups of chitosan with the zinc ions. The higher the pH the less positive the $–NH_3^+$ groups become. However, Ludox has slightly negative surface charge, even at acid pH [54]. The adsorption tests of Zn^{2+} on chitosan were carried out at various pH. Comparable amounts of Zn^{2+} were removed at the pH of 5 and 6. However, with a further increase of basicity, at pH 7 sudden growth in adsorption was observed [52]. This trend suggests that a part of Zn^{2+} precipitates as $Zn(OH)_2$ at the pH of 7 already clearly. On the one hand, Zn^{2+} is the predominant species at acidic pH; however, it is replaced by $Zn(OH)_2$ at pH 8–11 [55, 56]. On the other hand, pH 8 was regarded by another group [43] as the most appropriate for the investigation of Zn–chitosan complex. The concentration of Zn^{2+} is a crucial factor, which designates a border pH at which $Zn(OH)_2$ precipitates, as well as the concentration of adsorbent chitosan and deacetylation degree of chitosan. The concentration of Zn^{2+} was significantly lower, in above-mentioned studies [45, 56] as compared to those used in the presented work. For example, the concentration of chitosan-adsorbent and of Zn^{2+} were 10 mg/50 ml and 10 mg/L [56], respectively. The synthesis mixture for HS1_Zn4 carbon in this work usually contains ca. 0.5 g of chitosan in 100 ml of solution and ca. 0.9 g of $ZnCl_2{\cdot}H_2O$. To evaluate whether $Zn(OH)_2$ exists at even lower pH, the pH of the synthetic mixture of HS1_Zn4k was adjusted to 5.8. The TGA results for the HS1_Zn4pH5.8k sample were included in Fig. 10 b. At the pH of 5.8, some of the zinc species exist as cations, whereas others precipitate as $Zn(OH)_2$. Probably $Zn(OH)_2$ at 250 °C is transformed into ZnO (Fig. S5 includes XRD patterns of HS1_Zn4pH5.8 and HS1.38_Zn4pH5.8 carbons, which confirm that ZnO wurcite must have been formed above 200 °C and decomposes at least at 900 °C, Online Resource 1). The pure wurcite hexagonal phase was found in the XRD pattern [57]. Thermally removable, in-situ obtained from $Zn(CH_3COO)_2$, ZnO template have been used in the synthesis of N-doped carbon from polyvinylpyrrolidone [30].

An abundant peak at 380 °C can be associated with activation of semi-pyrolytic products by $ZnCl_2$. It appears at a lower temperature as compared to the decomposition of the

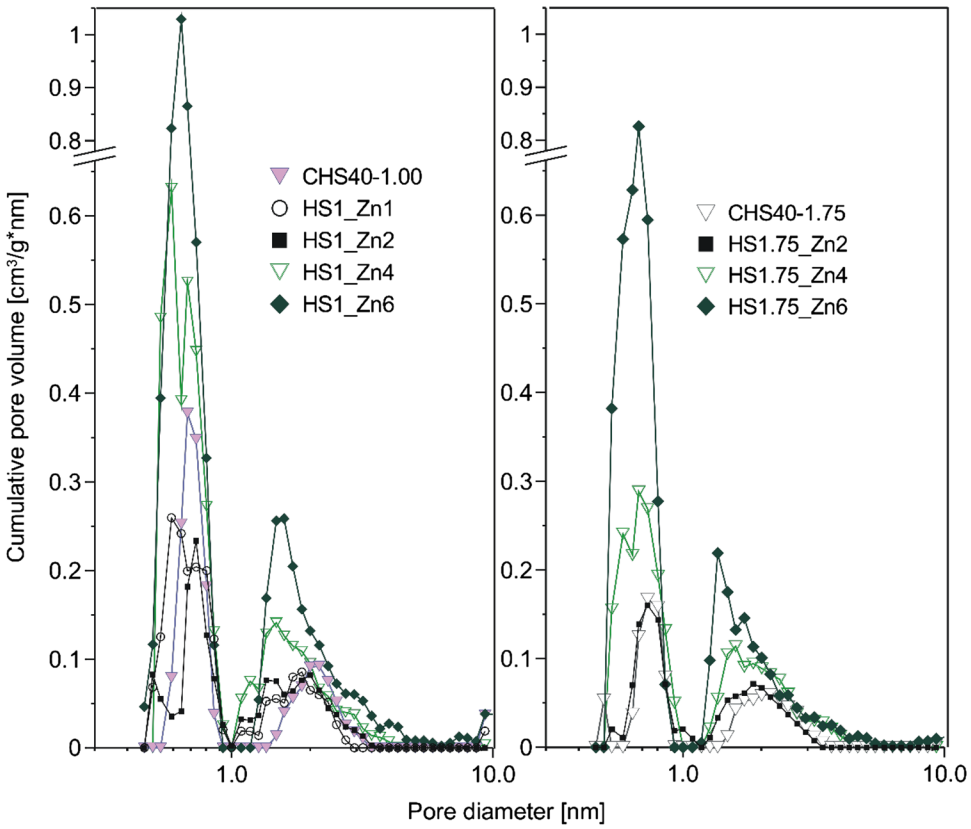

Fig. 7 Micro-mesoporous size distributions obtained by Do's method (optimized by ASA algorithm) for $ZnCl_2$ modified mesoporous carbons of HS1_ZnY (**a**) and HS1.75_ZnY (**b**) types. The results for parent samples (non-modified—CHS40-1.00 and CHS40-1.75, respectively), were presented for comparison

material prepared at lower pH of 3.9. Thus, the presence of ZnO accelerates further interaction of $ZnCl_2$ and char. A broad weight loss of ca. 21 wt%, observed within the range of temperature of 700–900 °C, can be attributed to the reaction of ZnO and carbon—ZnO + C = CO + Zn. The boiling point of metallic Zn is 907 °C. The XRD confirmed the ZnO, to be another activating agent during pyrolysis of gelatin [29] at the temperature higher than 670 °C. This reaction proceeds above 700 °C in the presented work. The carbonization temperature of 900 °C enables removal of ZnO from the structure which was supported by SEM/EDX results.

3.3 FTIR

There are the FTIR spectra of blends of: chitosan, chitosan–silica, chitosan–$ZnCl_2$, and chitosan–silica–$ZnCl_2$ composites in Fig. 11. Because of the fact, the stretching vibrations bands of N–H and O–H, (3100–3600 cm^{-1}) overlap with the Si–OH stretching vibration band, the reliable interpretation of this region is difficult. After the addition of silica to the chitosan–$ZnCl_2$ solution, the bands of 3364 and 3307 cm^{-1} in the spectrum of CH_Zn4 are shifted to 3396 and 3310 cm^{-1}, respectively, which supports interaction.

The spectrum of pure chitosan is characterized by the band of amide group, (C=O), (amide I) at 1655 and 1560 cm^{-1} (–NH–), (amide II) band, as well as with the band at 1590 cm^{-1} corresponding to the –N–H bending vibrations [45] of primary amine group [58, 59]. If the acetic acid played a role of the chitosan's solvent, obtained chitosan acetate films should be washed in ammonia water solution and methanol to remove acetate residues and obtain pure chitosan films [58]. Because of the fact, such a treatment may have changed interactions, e.g. between Zn^{2+} and chitosan, it was not applied, in this work. Thus, the examined materials may contain chitosan acetate. The strong band within a range of 1550–1600 cm^{-1} and a weak one at ca. 1400 cm^{-1} attributed to asymmetric and symmetric stretching vibrations of carboxylate anions can be distinguished, respectively. That band can be overlapped with $–CH_2$ scissoring vibrations band [60]. On the other hand, the (amide I) band should be hardly visible [61]. These bands of carboxylates appear possibly at 1569 and 1570 cm^{-1} in the spectra of chitosan–silica–zinc and chitosan–zinc composites, respectively and at 1416 cm^{-1} in both. There is a small band at 1707 cm^{-1} in the spectra of chitosan and chitosan–silica composite, which did not appear in the spectra of zinc-containing composites. Thus, the band, due to the C=O stretching vibrations of free carboxylic acids, indicates that acetic acid is going out from the chitosan acetic acid salt [62].

The amide II band, which occurs at 1556 cm^{-1} in the spectra of chitosan acetate sample, was shifted to 1558 cm^{-1} in the spectra of the silica–chitosan and zinc–chitosan

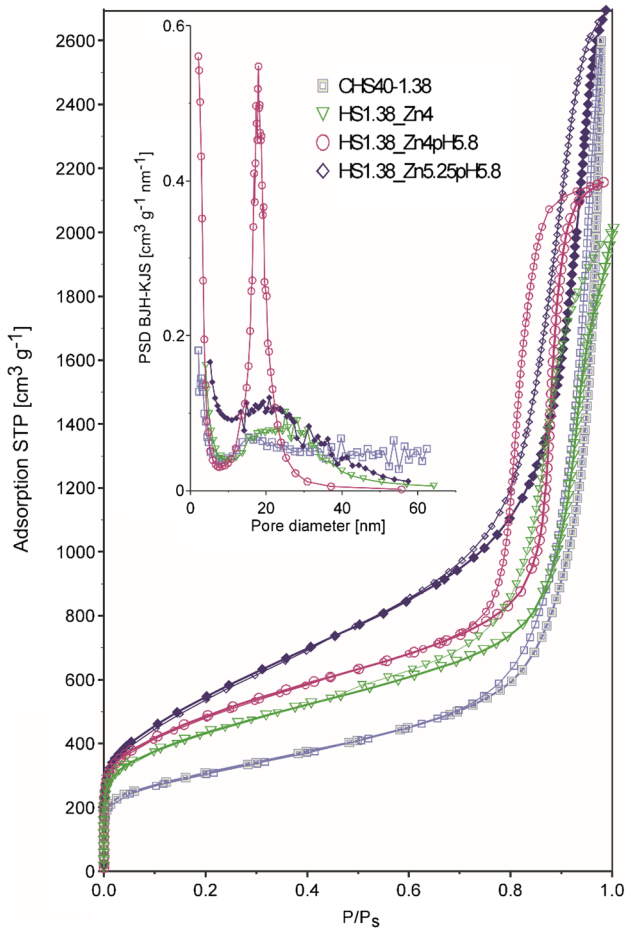

Fig. 8 Nitrogen sorption–desorption isotherms and BJH-KJS pore size distributions (adsorption) for CHS-40_1.38 sample modified with $ZnCl_2$ and obtained after the pH adjustement

composites. The bending vibrations of the amine group can be distinguished in the spectra of CH_Zn4 and HS1_Zn4k composites, as well—at 1614 and 1612 cm^{-1}, respectively. This band possibly is overlapped with the (amide I band) in the spectra of CH and CHS-1.00k. Moreover, the band of wagging –N–H vibrations mode at 656 cm^{-1} ,(which is very weak in the spectrum of CH_Zn4) is shifted to slightly higher wave number of 659 cm^{-1} in the chitosan–silica–zinc composite as opposite to band of second –OH group in chitosan (1051) to 1019 cm^{-1}. These shifts of the bands of –NH and OH groups, as well as a change of the position of the –NH bending vibrations band in the spectrum of chitosan–zinc composite (1614 cm^{-1}), after silica template incorporation (1612 cm^{-1}), confirms that groups of chitosan are involved in the coordination of the Zn^{2+} cation [45, 63]. The pH during synthesis of CH_Zn4 was 3.2–3.4 and increased up to 3.90 when silica was added (HS1_Zn4k). Wang et al. [64] revealed that at pH of 2 the amino groups of chitosan are fully protonated and the only interaction which exists among amino and hydroxyl groups of CH with the Zn ions is the chelation. However, with the pH increase, the interaction becomes more electrostatic [53]. The bands at 1380–1383 , 1318–1325 , and 1251–1255 cm^{-1} can be assigned to the deformation vibrations of methyl group [53], –CH wagging, $–CH_2$ twisting vibrations, [60] respectively. The last one and some of the bands described below, cannot be distinguished in the spectra of silica-containing composites, because of a broad band, which can be attributed to longitudinal optic Si–O–Si asymmetric (1170 cm^{-1}) and asymmetric stretching (1070 cm^{-1}) band [65] overlapping with it. The band situated at 950 cm^{-1} corresponds to vibrations of Si–OH groups, whereas that one around 800 cm^{-1} to v(M–O) stretching modes. The strong band at the wavelength of 472 cm^{-1} and a low frequency peak near 564 cm^{-1} can be attributed to Si–O–Si out of plane bending and Si–O–Si stretching modes, respectively [66]. The band observed in the range of 472–476 cm^{-1} was assigned to stretching vibrations of O–Zn [64]. The lack of this band in the spectrum of CH_Zn4 sample confirms the band at 472 cm^{-1} was above well attributed to Si–O–Si modes.

Further, the bands between 1148 and 896 cm^{-1} correspond to the polysaccharide skeleton. There are bands attributed to the vibrations of glycoside C–O bonds and stretching vibrations of C–O–C [53].

4 Conclusions

Well-ordered structure and high pore volume of CHS40 carbons are more sensitive to the silica content in a composite, as compared to the series obtained earlier, by using Ludox AS-40. Ordered porous structures are obtained for both templates with a silica-to-chitosan ratio from 1.0 to 2.5. However, at the silica-to-chitosan ratio of 2.5 for the CHS40_2.5 porous system is so strongly packed with silica, that it is difficult to remove it. A sample of 2.5 has already shown a slight effect of silica loading and its slightly thicker walls limit HF availability to the template. Isolation of the products of the reaction between precursor and $ZnCl_2$ during carbonization makes a further silica removal easier due to the already formed porous system.

The TEM/EDX results confirm uniform distribution of Zn^{2+} in the CHS40-1.00k composite. The results of thermal analysis and comparison of masses of samples before and after carbonization, confirm that the Zn^{2+} cations accelerate the decomposition of chitosan, even in the presence of the silica template present. The carbonization of the materials obtained at SiO_2/chitosan mass ratio of 1.38 and 1.75 and of those prepared in the presence of $ZnCl_2$ resulted in the slightly higher removal of nitrogen from the structure.

Addition of $ZnCl_2$ in a molar Zn-to-C (in chitosan mass) ratio of '4' increases the volume of micropores to 0.35 cm^3/g

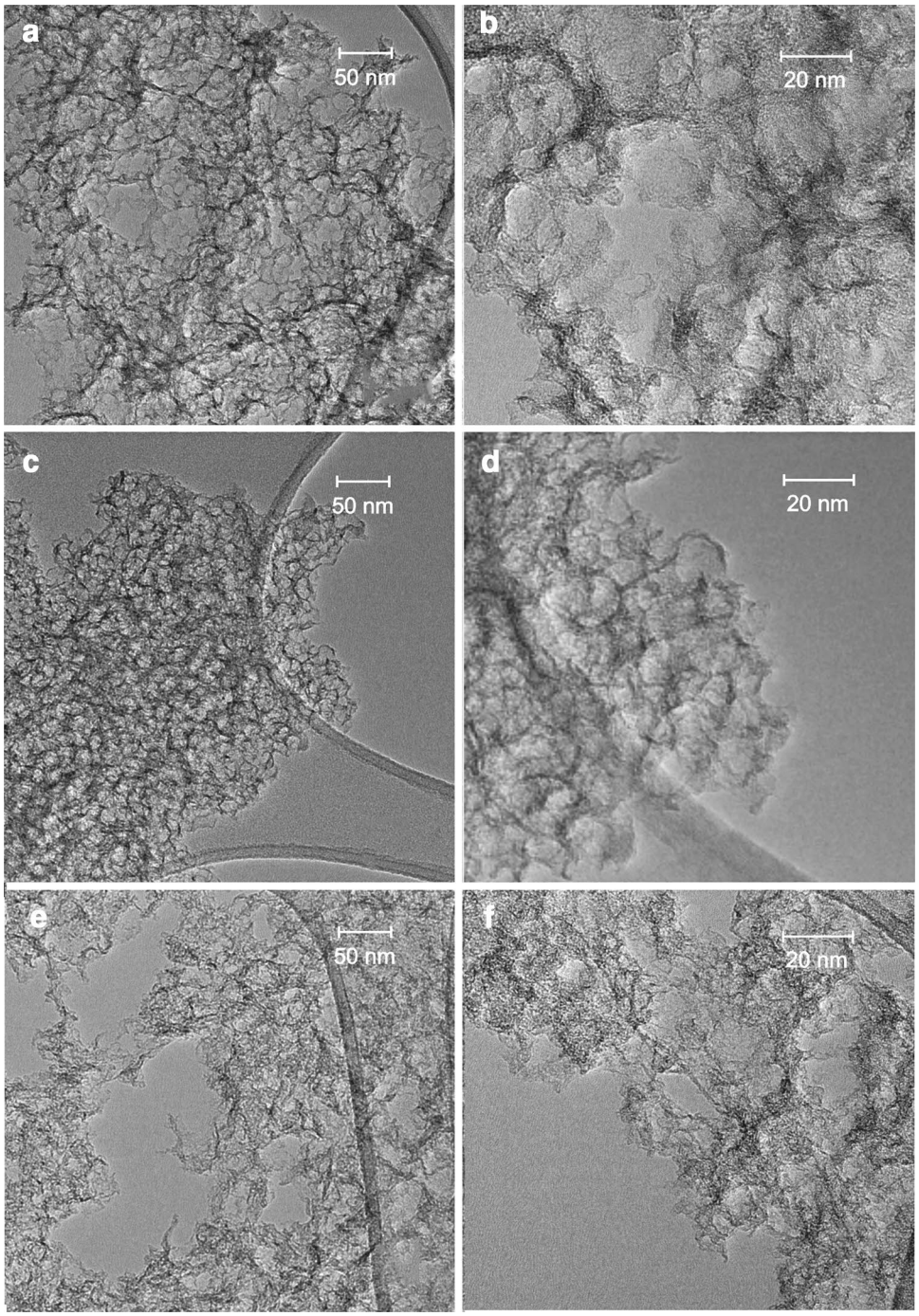

Fig. 9 TEM images of: HS1.38Zn4 (**a**, **b**), HS1.38Zn4pH5.8 (**c**, **d**), HS1.38Zn5.25pH5.8 (**e**, **f**)

and that of small mesopores, and in the case of the best sample (HS1.75_Zn4) the total V_{mes} of 2.41 cm^3/g, was slightly lower as compared to CHS40-1.75 carbon, which was characterized with V_{mes} of 2.91 cm^3/g. This was accompanied by a substantial development of the S_{BET} up to 1770 m^2/g. The ratio of 4.00 is similar to the mass ratio of ca. 1.42 and alike these found in the literature.

The pH of synthesis influences chitosan–Zn^{2+} interaction. The pH of the chitosan solution with zinc is low enough (ca 3.2–3.4) that the chitosan is too strongly protonated to co-ordinate with the groups of –OH and $–NH_2$. On the other hand, the increase in pH to 3.9 after addition of silica facilitates such coordination.

However, an increase of the pH up to 5.8 results in the precipitation of a new template—$Zn(OH)_2$ which is transformed during carbonization into ZnO. It was shown that, we can control the volumes of both micropores and small mesopores (of the diameter of ca. 3 nm) in the structure by using the appropriate amount of $ZnCl_2$ and suitable pH. The incorporation of $ZnCl_2$ into the synthesis mixture of silica template and carbon

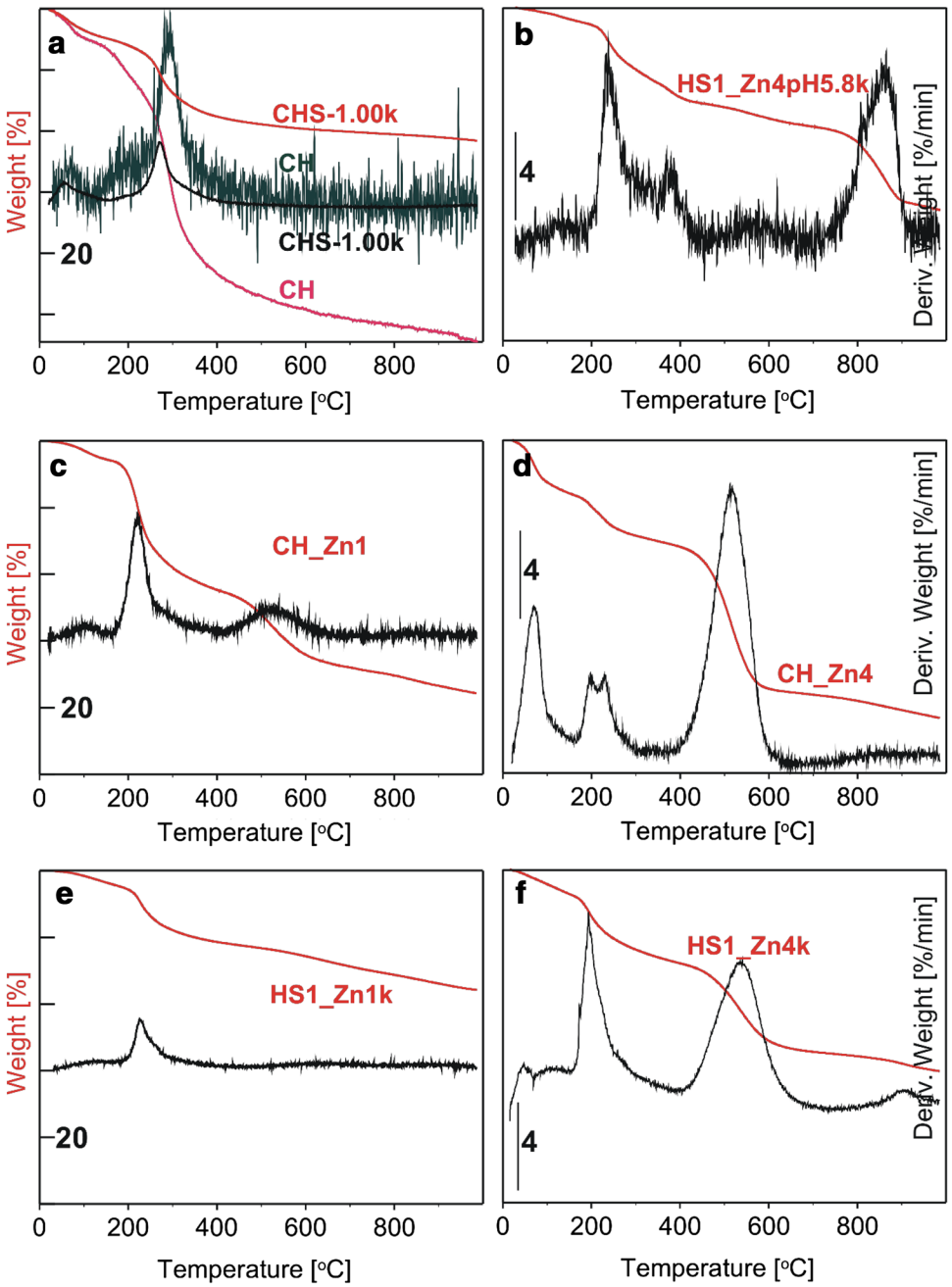

Fig. 10 TG and DTG curves of chitosan (CH, silica/chitosan) composite CHS-1.00 (**a**), chitosan-zinc composites without silica obtained at various zinc amounts (CH_Zn1 and CH_Zn4) (**c**, **d**), and of respective chitosan–zinc–silica composites in (**e**, **f**). The results for composite HS1_Zn4pH5.8 k prepared at pH 5.8 were presented in (**b**)

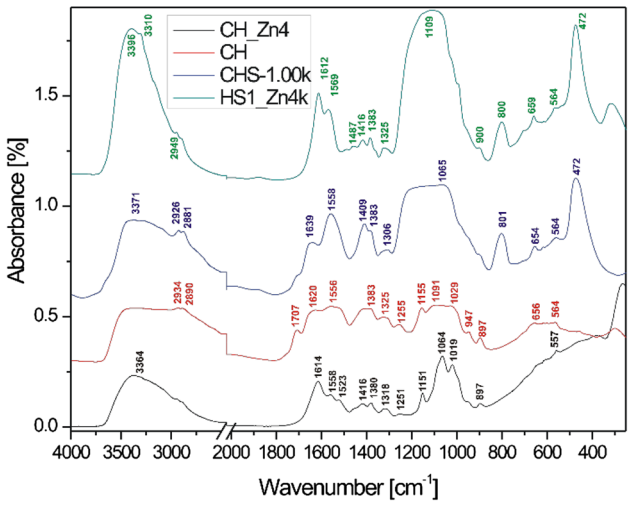

Fig. 11 FTIR spectra of chitosan, and chitosan–silica (CHS40_1.00k), chitosan–silica–zinc (HS1_Zn4k), and chitosan–zinc (CH_Zn4) composites

precursor is a strategy, which enables pH adjustment, and, in this case the in-situ synthesis of the new template.

Compliance with ethical standards

Conflict of interest The authors declare no conflict of interest.

References

1. D.W. Wang, F. Li, M. Liu, G.Q. Lu, H.M. Cheng, Angew. Chem. **120**, 379 (2008)
2. G. Lota, K. Fic, E. Frackowiak, Energy Environ. Sci. **4**, 1592 (2011)
3. J. Choma, J. Górka, M. Jaroniec, Microporous Mesoporous Mater. **19**, 1 (2007)
4. C. Liang, S. Dai, J. Am. Chem. Soc. **128**, 5316 (2006)
5. S.H. Joo, R. Ryoo, M. Kruk, M. Jaroniec, J. Phys. Chem. B **106**, 4640 (2002)
6. S. Han, T. Hyeon, Carbon **37**, 1645 (1999)
7. K.P. Gierszal, M. Jaroniec, J. Am. Chem. Soc. **128**, 10026 (2006)
8. J. Yu, M. Guo, F. Muhammad, A. Wang, F. Zhang, Q. Li et al., Carbon **69**, 502 (2014)
9. D. Liu, J.-H. Lei, L.-P. Guo, K.-J. Deng, Carbon **49**, 2113 (2011)
10. D. Liu, C. Zeng, D. Qu, H. Tang, Y. Li, B.-L. Su et al., J. Power Sources **321**, 143 (2016)
11. J. Choma, W. Fahrenholz, D. Jamioła, J. Ludwinowicz, M. Jaroniec, Microporous Mesoporous Mater. **185**, 197 (2014)
12. M.K. Sahoo, P. Gogoi, G. Rajeshkhanna, S.V. Chilukuri, G. Ranga Rao, Appl. Surf. Sci. **418**, 40 (2016)
13. C. Pevida, T.C. Drage, C.E. Snap, Carbon **46**, 1464 (2008)
14. B.E. Wilson, S. He, K. Buffington, S. Rudisill, W.H. Smyrl, A. Stein, J. Power Sources **298**, 193 (2015)
15. M.K. Rybarczyk, M. Lieder, M. Jablonska, RSC Adv. **5**, 44969 (2015)
16. J. Wang, H. Chen, H. Zhou, X. Liu, W. Qiao, D. Long, L. Ling, J. Environ. Sci. **25**, 124 (2013)
17. JL. Estevez, R. Dua, N. Bhandari, A. Ramanujapuram, P. Wang, E.P. Giannelis, Energy Environ. Sci. **6**, 1785 (2013)
18. N. Bhandari, R. Dua, L. Estevez, R. Sahore, E.P. Giannelis, Carbon **87**, 29 (2015)
19. M. Jaroniec, J. Gorka, J. Choma, A. Zawislak, Carbon **47**, 3034 (2009)
20. J.H. Bang, H.-M. Lee, K.-H. Anc, B.-J. Kim, Appl. Surf. Sci. **415**, 61 (2017)
21. K. Xia, Q. Gao, J. Jiang, J. Hu, Carbon **46**, 1718 (2008)
22. E. Raymundo-Piñero, K. Kierzek, J. Machnikowski, F. Beguin, Carbon **44**, 2498 (2006)
23. L. Zubizarreta, A. Arenillas, J.-P. Pirard, J.J. Pis, N. Job, Microporous Mesoporous Mater. **115**, 480 (2008)
24. A.C. Lua, T. Yang, J. Coll. Interf. Sci. **290**, 505 (2005)
25. Z. Hu, M.P. Srinivasan, Microporous Mesoporous Mater. **43**, 267 (2001)
26. Z. Hu, M.P. Srinivasan, Y. Ni, Carbon **39**, 877 (2001)
27. N.R. Khalili, M. Campbell, G. Sandi, J. Golaś, Carbon **38**, 1905 (2000)
28. B.K. Mazumdar, D.D. Banerjee, G. Ghosh, Energy Fuels **2**, 224 (1988)
29. S. Yu, H. Wang, C. Hu, Q. Zhu, N. Qiao, B. Xu, J. Mater. Chem. A **4**, 16341 (2016)
30. S. Wang, Z. Cui, J. Qin, M. Cao, Nano Res. **9**, 2270 (2016)
31. X.-L. Dong, A.-H. Lu, B. He, W.-C. Li, J. Power Sources **327**, 535 (2016)
32. A. Olejniczak, M. Leżańska, J. Włoch, A. Kucińska, J.P. Lukaszewicz, J. Mater. Chem. A **1**, 8961 (2013)
33. M. Lezanska, A. Olejniczak, A. Pacula, G. Szymanski, J. Wloch, Catal. Today **227**, 223 (2014)
34. M. Kruk, M. Jaroniec, A. Sayari, Langmuir **13**, 6267 (1997)
35. C. Nguyen, D.D. Do, Langmuir **16**, 1319 (2000)
36. A.P. Terzyk, P.A. Gauden, P. Kowalczyk, Carbon **40**, 2879 (2002)
37. P.A. Gauden, P. Kowalczyk, A.P. Terzyk, Langmuir **19**, 4253 (2003)
38. M. Thommes, K. Kaneko, A.V. Neimark, J.P. Olivier, F. Rodriguez-Reinoso, J. Rouquerol, K.S.W. Sing (2015) Physisorption of gases, with special reference to the evaluation of surface area and pore size distribution (IUPAC Technical Report). Pure Appl. Chem. 87(9–10):1051–1069
39. M. Kruk, M. Jaroniec, K.P. Gadkaree, J. Colloid. Interf. Sci. **192**, 250 (1997)
40. F. Caturla, M. Molina-Sabio, F. Rodriguez-Reinoso, Carbon **29**, 999 (1991)
41. M. Kruk, C.M. Hui, Microporous Mesoporous Mater. **114**, 64 (2008)
42. P.J. Ravikovitch, A.V. Neimark, Langmuir **18**, 9830 (2000)
43. J.C. Groen, L.A.A. Peffer, J. Perez-Ramirez, Microporous Mesoporous Mater. **60**, 1 (2003)
44. E. Szymanska, K. Winnicka, Mar. Drugs **13**, 1819 (2015)
45. C. Ou, S. Chen, Y. Liu, J. Shao, S. Lib, T. Fuc et al., J Anal. Appl. Pyrol. **122**, 268 (2016)
46. L. Zeng, C. Qin, L. Wang, W. Li, Carbohydr. Polym. **83**, 1553 (2011)
47. G.R. Ponder, G.N. Richards, Biomass Bioenergy **7**, 1 (1994)
48. H. Kaczmarek, J. Zawadzki, Carbohydr. Res. **345**, 941 (2010)
49. G.Z. Kyzas, M. Kostoglou, T. Lazaridis, Chem. Eng. J. **152**, 440 (2009)
50. Y. Higashio, T. Shoji, Appl. Catal. A **260**, 251 (2004)

51. Material Safety Data Sheet of Zinc Chloride (nr 229997) Sigma-Aldrich (Merck KGaA) in Poland
52. K.D. Trimukhe, A.J. Varma, Carbohydr. Polym. **75**, 63 (2009)
53. G.Z. Kyzas, P.I. Siafaka, E.G. Pavlidou, K.F. Chrissafis, D. Bikiaris, Chem. Eng. J. **259**, 438 (2015)
54. W. R. Grace & Co.-Conn,Ludox® colloidal silica. (Grace Davison Technical Information, 2008), https://grace.com/general-industrial/enus/Documents/ludox_binders%20refractory_E_08_081110.pdf. Accessed 21 June 2017
55. W.P. Cunningham, *Environmental Encyclopedia*, 2nd edn. (Jaia, Chennai, 1999)
56. G. Karthikeyan, K. Anbalagan, N. Muthulakshmi Andal, J. Chem. Sci. **116**, 119 (2004)
57. XRD pattern of hexagonal ZnO JCPDS Card No. 36–1451
58. M. Mucha, Polimery **47**, 509 (2002)
59. M. Kaya, I. Akata, T. Baran, A. Mentes, Food Biophys. **10**, 162 (2015)
60. J. Kowalonek, Int. J. Biol. Macromol. **103**, 515 (2017)
61. J. Nunthanid, M. Laungtana-anan, P. Sriamornsak, S. Limmatvapirat, S. Puttipatkhachorn, L.Y. Lim, E. Khor, J. Control. Release. **99**, 15 (2004)
62. Z. Osman, Electrochim. Acta **48**, 993 (2003)
63. N.-S.H. David, L.G. Tang, J. Appl. Polym. Sci. **77**, 2246 (2000)
64. X. Wang, Y. Du, H. Liu, Carbohydr. Polym. **56**, 21 (2005)
65. O. Gutiérrez-Arriaga, S.R. Vásquez-García, N. Flores-Ramírez, G. Luna-Bárcenas, G. Barrera-Cardiel, C.A. León-Patiño, Global J. Sci. Front. Res. Chem. **12**, 1 (2012)
66. R.K. Nariyal, P. Kothari, B. Bisht, Chem. Sci. Trans. **3**, 1064 (2014)